Measurement of the Q value of an acoustic resonator

Tetsushi Biwa, Yuki Ueda, Hiroshi Nomura, and Uichiro Mizutani
Department of Crystalline Materials Science, Nagoya University, Nagoya 464-8603, Japan

Taichi Yazaki
Department of Physics, Aichi University of Education, Kariya, 448-8542, Japan
(Received 16 December 2004; published 1 August 2005)

A cylindrical acoustic resonator was externally driven at the first resonance frequency by a compression driver. The acoustic energy stored in the resonator and the power dissipated per unit time were evaluated through the simultaneous measurements of acoustic pressure and velocity, in order to determine the Q value of the resonator. The resulting Q value, being employed as a measure of the damping in a resonator, was obtained as 36. However, the Q value determined from a frequency response curve known as a conventional technique turned out to be 25, which is 30% less than that obtained in the present method. By further applying these two methods in the case of a resonator having an acoustic load inside, we present an accurate measurement of the Q value of the resonator by making full use of its definition.

DOI: 10.1103/PhysRevE.72.026601 PACS number(s): 43.58.+z, 47.40.−x, 43.35.+d

I. INTRODUCTION

Resonance is the phenomenon that is commonly observed in various physical systems like a forced pendulum and electrical circuits, and is generally characterized by a resonance frequency f_0 and a quality factor called the Q value. The Q value is defined as

$$Q = 2\pi f_0 \frac{E_S}{\dot{E}}, \tag{1}$$

where E_S represents the energy stored in the system and $\dot{E}$ the energy loss per unit time when the system is driven at f_0.

The resonant oscillation reaches the steady state when the energy loss $\dot{E}$ associated with the oscillation becomes equal to the input power supplied from the driver. In an ideal system without any dissipations, E_S should increase infinitely upon the application of even an infinitesimally small input power. Hence, the Q value obviously tends to infinity. In contrast, the Q value in a real system would remain finite as a result of unavoidable dissipative processes. Thus, the Q value can be employed as a measure to judge the degree of damping in a driven system.

In many physical systems such as nuclear magnetic resonance, the Q value is conventionally obtained from a frequency response curve. In acoustics, for example, the acoustic pressure in the acoustic resonator is measured as a function of the driving frequency f [1]. The frequency response curve in this case refers to the relation between the squared pressure and f. The Q value is derived from the curve as the ratio of the resonance frequency f_0 to the difference Δf between half-power frequencies. It is extremely simple for experimentalists to determine the Q value from the response curve. However, it is sometimes forgotten that the oscillating velocity of a driver piston must be fixed regardless of f [1,2], which is the awkward and challenging driving condition required in this method.

Recent progress in the study of thermoacoustics has made it possible to accurately measure the acoustic intensity I through simultaneous measurements of the acoustic pressure $P=p\exp(i\omega t)$ and acoustic particle velocity $U=u\exp\{i(\omega t+\Phi)\}$, the latter being measured with a laser Doppler velocimetry (LDV) [3–5], where ω represents the angular frequency ($=2\pi f$). The acoustic intensity I is given as

$$I = \langle PU \rangle_t, \tag{2}$$

where angular brackets $\langle \cdots \rangle_t$ represent a time average of the internal quantity PU. The acoustic intensity I or the acoustic power flux per unit area in units of $\mathrm{W/m^2}$ has been measured to determine the output power of a thermoacoustic engine [3,6–9]. This technique to determine I also enables the evaluation of the input power from the driver, which is equal to the dissipative power $\dot{E}$ in the resonator. It is also possible to determine the acoustic energy E_S stored in the resonator from the measurements of the axial distribution of P and U.

The present work reports on accurate measurements of the Q value of the acoustic resonator by making full use of its definition in Eq. (1). The energy E_S stored in the resonator and the input power $\dot{E}$ entering the resonator were obtained through the simultaneous measurements of P and U in a cylindrical acoustic resonator driven at the first resonance frequency. By inserting E_S and $\dot{E}$ into Eq. (1), the Q value of the resonator was directly determined, which is significantly different from the Q value evaluated by means of the conventional method using a frequency response curve. By further applying these two methods to the resonator having an acoustic load inside, we show that the present method provides the Q value relevant only to the resonator, whereas the conventional method gives the Q value in the combined driver-resonator system.

II. EXPERIMENTAL METHOD

A. Acoustic resonator

The present experimental apparatus is schematically shown in Fig. 1. An acoustic resonator was made of a Pyrex

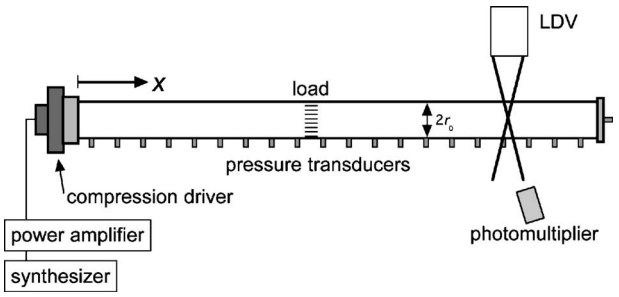

FIG. 1. Schematic illustration of a present acoustic resonator. The normalized axial coordinate X is directed from the acoustic driver to a closed end. A ceramic catalyst is inserted at $X=0.46$ as an acoustic load.

glass cylinder with length $L=1.02$ m and inner radius $r_0=10.5$ mm. The working fluid is atmospheric air. One end of the resonator was closed by a rigid plate, and the other was connected to a compression driver (Electro Voice 1829B). The constant-voltage signal from a synthesizer was sent through a power amplifier to the driver in the frequency range 135–165 Hz.

The measurements of the Q value were made in this simple resonator with and without an acoustic load. A 2-cm-long cylindrical ceramic catalyst, which is of a right size to fit into the glass tube, was inserted into the resonator as the acoustic load. This catalyst has many square holes with the side of 0.7 mm. The value of the parameter $\omega\tau_\nu$, which is introduced in the next section, is 3.8 in the load and 3430 in the glass tube region.

The pressure amplitude p_e at the rigid end of the resonator was measured while varying the driving frequency f. The frequency response curve thus obtained is plotted in Fig. 2, where p_e is normalized with respect to $p^*=782$ Pa. It is found that the peak is formed at 148.5 Hz, which corresponds to the fundamental resonance frequency f_0 in the present system. The full width Δf at a half maximum was determined as 5.8 Hz by fitting the response curve to a Lorentz curve. Thus, the Q value $Q_f=f_0/\Delta f$ obtained from the frequency response curve turned out to be 25. This is the conventional derivation of the Q value of the resonator, taking aside the nuisance that the driver velocity might depend on f even with the constant voltage suppiled to the driver [2].

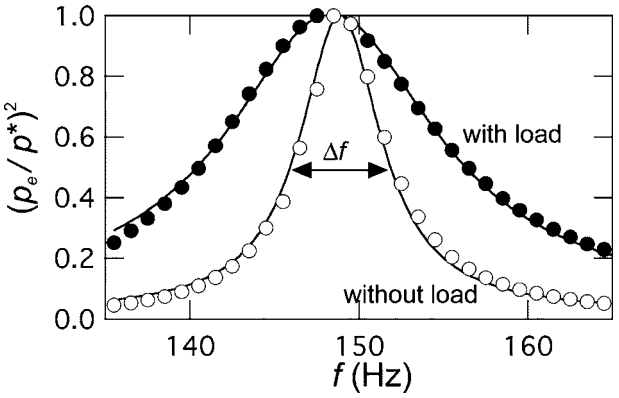

FIG. 2. Frequency response curve of a present resonator. Solid and open circles represent the square of the normalized pressure $(p_e/p^*)^2$ at the closed end of the resonator with and without the load, respectively, where $p^*=782$ Pa.

As a next step, we installed the ceramic catalyst at the velocity antinode formed in the middle of the resonator and measured the frequency response curve of the loaded resonator. The quality factor Q_f of the loaded resonator was determined to be 9.9 from the response curve shown by solid circles in Fig. 2. These Q values with and without the load will be compared with the Q values determined by using Eq. (1).

B. Pressure and velocity measurement

We measured pressure $P=p\exp(i\omega t)$ using small pressure transducers, which were mounted in the glass tube wall via short ducts of 1 mm in radius and 10 mm in length [5]. Since the wavelength of the acoustic wave is much longer than r_0 in the present experiments, the pressure P is safely assumed to be spatially uniform over the cross section of the tube. However, the axial acoustic particle velocity $U(r)=u(r)\exp[i\{\omega t+\Phi(r)\}]$ depends on a radial coordinate r in a cylinder because of the viscosity of the gas. A LDV was used for the measurements of $U(r)$. We took into account a time lag $(2.7\times10^{-5}$ S) induced by a tracker-type processor to determine precisely the phase of the velocity. Pressure and velocity signals were simultaneously recorded with a multichannel 24-bit spectrum analyzer. We obtained the amplitudes p and $u(r)$ and the phase lead $\Phi(r)$ of $U(r)$ relative to P from power and phase spectra, respectively.

The radial distribution of the velocity $U(r)$ is governed by a nondimensional parameter $\omega\tau_\nu$ [10] as derived from a laminar flow theory. Here the parameter τ_ν represents the relaxation time expressed as $r_0^2/(2\nu)$, where ν is the kinematic viscosity of the fluid. The parameter $\omega\tau_\nu$ is related to the viscous boundary layer thickness $d=\sqrt{2\nu/\omega}$ a

$$\omega\tau_\nu=\left(\frac{r_0}{d}\right)^2. \tag{3}$$

Figure 3(a) shows the radial distribution of U when the parameter $\omega\tau_\nu=39$ is achieved in a cylindrical tube similar to that shown in Fig. 1. The amplitude u and phase lead Φ relative to P are plotted as a function of the normalized radial coordinate $r_n=r/r_0$. We see that both the amplitude u and phase lead Φ change greatly in the viscous boundary layer near the wall. Since the viscous stress is proportional to $\mu\nabla_r^2U$, we see that the viscous dissipation takes place quite locally in the region within about $3d$ from the tube wall, where μ denotes dynamic viscosity of the gas and ∇_r^2 represents the radial component of the Laplacian. On the other hand, both u and Φ are almost independent of r_n in the core region $r_n<1-3d/r_0$. This means that viscous loss is ignored in the core region.

We also measured U when $\omega\tau_\nu=4.0$ and 470. The value of $\omega\tau_\nu=4.0$ is quite close to that (=3.8) in the acoustic load employed in the present work. As shown in Fig. 4(a), u shows a parabolic profile similar to the Hagen-Poiseuille flow in a steady laminar flow [11] when $\omega\tau_\nu$ is 4.0. Since the viscous boundary layer thickness d extends more than half of

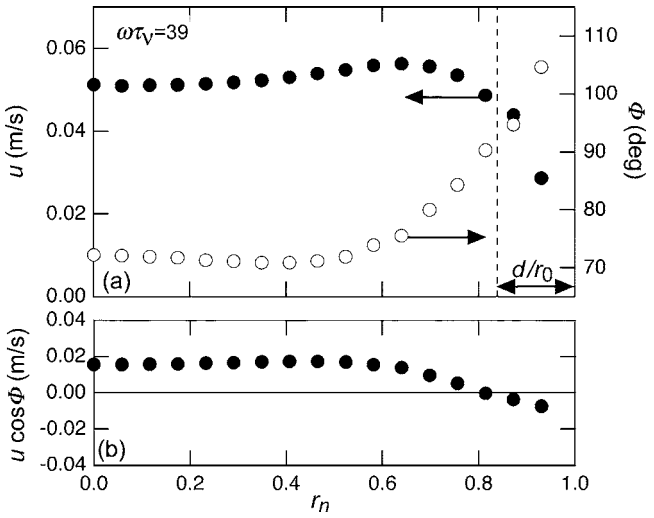

FIG. 3. Radial profile of the axial particle velocity when $\omega\tau_\nu = 39$. Experimental data of the velocity amplitude u (solid markers) and the phase lead Φ relative to pressure P (open markers) are shown in (a), and the traveling-wave component $u\cos\Phi$ is shown in (b). Data are shown as a function of a normalized radial coordinate r/r_0 taken from the central axis of the tube toward the wall. A vertical line in (a) is drawn at d/r_0 away from the tube wall.

the cross-sectional area of the tube, the viscous dissipation becomes significant. On the other hand, when $\omega\tau_\nu$ is 470, u and Φ are almost uniform over the cross section because of the smallness of d relative to r_0, as shown in Fig. 4(b). In the present acoustic resonator, $\omega\tau_\nu$ is given as 3430 in the glass tube region, which leads to $d/r_0 = 0.017$. Consequently, the

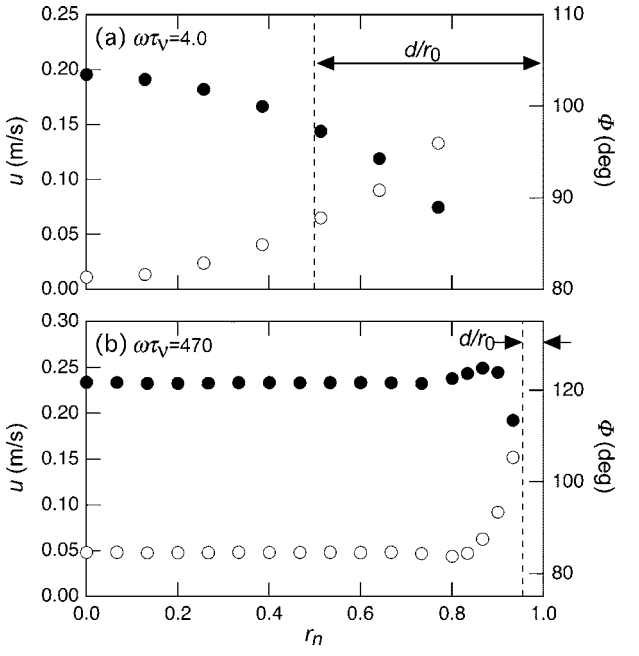

FIG. 4. Radial profile of the axial particle velocity when (a) $\omega\tau_\nu = 4.0$ and (b) $\omega\tau_\nu = 470$. The velocity amplitude u and the phase lead Φ relative to pressure P are shown by solid and open markers, respectively. Vertical lines are drawn at d/r_0 away from the tube wall.

radial distribution of u and Φ shows a flat profile almost in the entire cross section of the tube.

C. Acoustic intensity measurement

The acoustic intensity $I(r)$ defined in Eq. (2) is rewritten as $I(r) = \langle PU(r)\rangle_t = (1/2)pu(r)\cos\Phi(r)$. This is the local acoustic power flux and is obviously dependent on the radial coordinate of the tube. Since p is independent of r, the radial dependence of $I(r)$ is governed by a factor $u(r)\cos\Phi(r)$ called a traveling-wave component (TWC) of U [6–8]. As shown in Fig. 3(b), the TWC is positive in the central region of the tube but becomes negative in the viscous boundary layer. This indicates that I near the wall flows in the direction opposite to that in the central region. This would result in an r-dependent mass streaming due to the oscillatory motion of the gas [9,12].

We focus on the cross-sectional average $\bar{I}$ of the acoustic intensity $I(r)$, which is expressed as

$$\bar{I} = \overline{\langle PU(r)\rangle_t}, \tag{4}$$

where an overbar represents the cross-sectional average. By taking the cross- sectional average prior to the temporal average of the product $PU(r)$, we obtain

$$\bar{I} = \langle PV\rangle_t = \frac{1}{2}pv\cos\phi, \tag{5}$$

where $V = v\exp\{i(\omega t + \phi)\}$ represents the cross-sectional mean of $U(r)$. We can obtain the cross-sectional mean velocity V from the measured velocity $U(0) = u(0)\exp[i\{\omega t + \Phi(0)\}]$ on the central axis of the tube. The laminar flow theory [10] links $U(0)$ with V through the relations

$$v = u(0)/\Gamma, \tag{6}$$

$$\phi = \Phi(0) - \Psi, \tag{7}$$

where Γ and Ψ are analytically given as a function of $\omega\tau_\nu$, respectively.

Figures 5(a) and 5(b) show Γ and Ψ calculated for a circular cylinder. The theoretical factors Γ and Ψ approach unity and zero, respectively, when $\omega\tau_\nu$ is very large. This is because the velocity $U(r)$ becomes uniform over the cross section, as we have stressed in the previous section. However, Γ reaches 2 when $\omega\tau_\nu$ is small, whereas Ψ shows a minimum at $\omega\tau_\nu = 14$. In the present experiment, $\omega\tau_\nu$ is equal to 3430 in the resonator and $\Gamma = 1.0$ and $\Psi = -1.0°$ are used, respectively. The factor $\Psi = -1.0°$ seems to be small, but it is very important for the precise measurements of $\bar{I}$ in an acoustic resonator, as we will show later.

In addition to the factors Γ and Ψ, we should also take into account the accuracy in the measurement of $U(0)$. When $\omega\tau_\nu$ is very large, the boundary layer thickness d becomes very small compared to the tube radius. Under such a condition, we can measure the core velocity $U(0)$ accurately even when the actual position of the LDV probe is far off from the central axis of the tube. However, when $\omega\tau_\nu$ is small, even a slight difference in the radial position of the LDV probe from

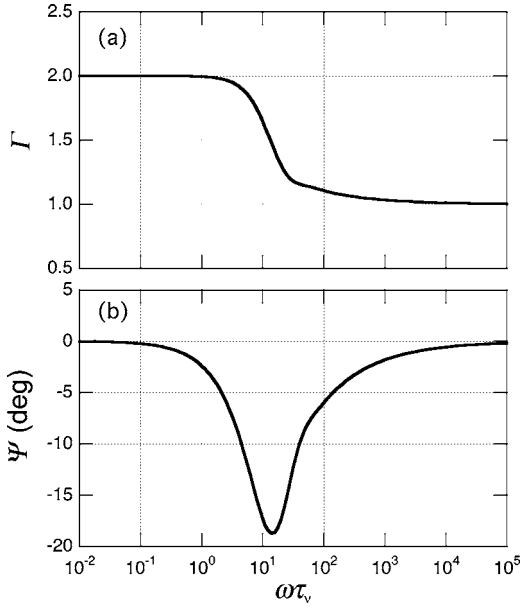

FIG. 5. The $\omega\tau_\nu$ dependence of theoretical factors (a) Γ and (b) Ψ, which represent the amplitude ratio and the phase lead of the core velocity $U(0)$ relative to the cross-sectional mean velocity V, respectively.

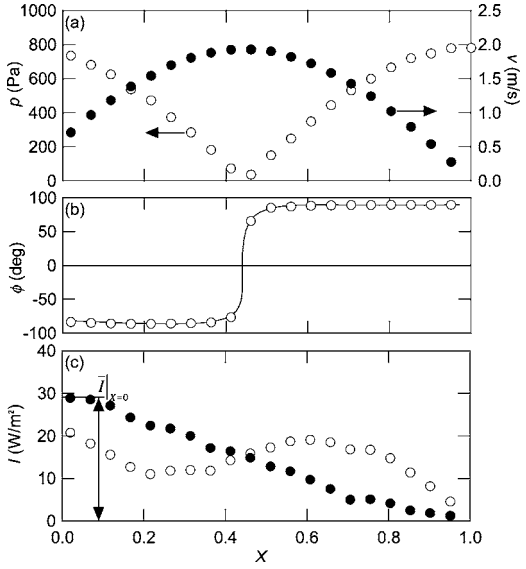

FIG. 6. Acoustic field in the present resonator. Axial profile of (a) pressure p and velocity v, (b) the phase lead ϕ of V to P, and (c) the acoustic intensity $\bar{I}$. Open markers in (c) represents the acoustic intensity determined without taking into account the corrections of the phase ϕ.

the center line results in a large error in the measurements of $U(0)$ and hence $\bar{I}$.

D. Acoustic intensity in a resonator

The present resonator shown in Fig. 1 was driven at the fundamental resonance frequency $f_0=148.5$ Hz, and the pressure p_e at the rigidly closed end was adjusted to $p^*=782$ Pa. Figures 6(a) and 6(b) show the axial distribution of p, v, and ϕ in the resonator. The axial coordinate X represents the distance from the driver and is normalized with respect to the total length L of the resonator. Since the fundamental mode is excited in the resonator, the pressure amplitude p takes two maxima—i.e., one at the closed end and the other in front of the acoustic driver—whereas v shows a maximum at $X=0.46$. The phase ϕ is very close to a standing-wave phase ($=90°$) except the position of the velocity maximum at $X=0.46$, where it becomes a traveling-wave phase ($=0°$).

We determined the axial distribution of $\bar{I}$ by inserting p, v, and ϕ shown in Figs. 6(a) and 6(b) into Eq. (4). As shown in Fig. 6(c), the acoustic intensity $\bar{I}$ is positive throughout the resonator. This represents the fact that $\bar{I}$ flows from the driver to the closed end. The acoustic intensity $\bar{I}|_{X=0}$ emitted from the driver at $X=0$ is found to be 29 W/m^2. The acoustic intensity $\bar{I}$ monotonically decreases to zero at the closed end as it flows down. A negative slope $\nabla\bar{I}$ represents the local dissipative power per unit volume due to thermal conduction and viscosity of the gas oscillating in the vicinity of the wall. The local dissipative power $\nabla\bar{I}$ varies as a function of X, and we see that $\nabla\bar{I}$ is $\bar{I}|_{X=0}/L\approx 29$ W/m^3 as the spatial average over the resonator.

The measuring uncertainty $\delta\bar{I}$ of the acoustic intensity $\bar{I}$ is estimated from the expression

$$\left|\frac{\delta\bar{I}}{\bar{I}}\right| \approx \left|\frac{\delta v}{v}\right| + \left|\frac{\delta p}{p}\right| + |\delta\phi \tan\phi|, \tag{8}$$

where δv, δP, and $\delta\phi$ represent respective uncertainties in v, p, and ϕ. The error $\delta\bar{I}$ was typically 1.0 W/m^2, which is of the size of symbols in Fig. 6(c). The error $\delta\bar{I}$ arises mainly from the third term on the right-hand side of Eq. (8), where $\delta\phi=0.2°$.

In evaluating $\bar{I}$, we had carefully determined the phase lead ϕ by taking into account all time lags originating from the instruments and also the phase difference Ψ between $U(0)$ and V. For comparison, we plotted the acoustic intensity without making any correction in the phase ϕ by open circles in Fig. 6(c). The acoustic intensity without the correction shows a positive slope in the region $0.2<X<0.6$. This is physically unacceptable because there is no acoustic power amplifier such as a differentially heated regenerator [6–9,13,14]. This means that a small deviation in ϕ from a standing wave phase ($=90°$) plays an important role in producing the axial distribution of $\bar{I}$ shown in Fig. 6(c). Therefore, great attention should be paid to determine the value of $\Phi(0)$ and Ψ when ϕ is close to a standing-wave phase.

III. RESULTS AND DISCUSSION

A. Q value of an acoustic resonator

The acoustic intensity $\bar{I}$ of the tube represents the cross-sectional average of the dynamic power flux per unit area due to the oscillating gas. Hence, the acoustic power flow is

given by the product of the cross-sectional area of the resonator and $\bar{I}$. The acoustic power flow decreases as it flows down by the dissipative processes in the resonator, as we have seen in the previous section. Therefore, the energy loss $\dot{E}$ in the resonator is given by the total decrease of the acoustic power flow as

$$\dot{E} = \int_L^0 \pi r_0^2 \nabla \bar{I} dX = \pi r_0^2 \bar{I}|_{X=0}. \tag{9}$$

As a result, we obtain $\dot{E}=1.0\times10^{-3}$ W.

The acoustic energy density e_d is the sum of the acoustic potential-energy density and the acoustic kinetic-energy density [15]. Since $\omega\tau_\nu \gg 1$ in the present resonator, the acoustic energy density e_d is expressed as

$$e_d = \frac{1}{4}\left(\frac{p^2}{\rho a^2} + \rho v^2\right), \tag{10}$$

where ρ and a represents the mean density and the adiabatic sound speed, respectively. The experimental evaluation of e_d is easily made in good precision because e_d is given only by the amplitudes p and v and has nothing to do with the phase ϕ. The total acoustic energy E_S stored in the resonator is given as the volume integral of e_d. Since a standing-wave field is excited in the present resonator, E_S is given as

$$E_S = \int_{resonator} e_d dV = \pi r_0^2 L \frac{p_{max} v_{max}}{4a}, \tag{11}$$

where p_{max} and v_{max} represent the maximum amplitude of pressure ($=p^*$) and velocity in the resonator. We found $E_S=0.39$ mJ by inserting the experimental data into Eq. (11). Now we are ready to determine the Q value of the acoustic resonator by using Eq. (1). The substitution of E_S and $\dot{E}$ thus determined into Eq. (1) yields $Q=36$ in the present resonator. This is the Q value relevant to the gas column in the resonator.

The dissipative power $\dot{e}$ per unit of surface area of the resonator is given from the linear acoustic theory [15] as

$$\dot{e} = \frac{\omega d}{4}\left(\frac{p^2(\gamma-1)}{\rho a^2\sqrt{\sigma}} + \rho v^2\right), \tag{12}$$

where γ and σ are the ratio of isobaric to isochoric specific heats and Prandtl number, respectively. The first and second terms correspond to the thermal and viscous attenuations at the resonator wall. The energy loss $\dot{E}$ in the resonator is then given by the integration of $\dot{e}$ over the surface of the resonator. Since the standing-wave field is excited in the resonator, we have

$$\dot{E} = \pi r_0^2 L \frac{p_{max} v_{max}}{4a}\sqrt{\frac{\omega}{\tau_\nu}}\left(1 + \frac{\gamma-1}{\sqrt{\sigma}}\right). \tag{13}$$

By substituting Eqs. (11) and (13) into Eq. (1), we obtain the theoretical Q_{th} as

$$Q_{th} = \frac{\sqrt{\omega\tau_\nu}}{1.5}, \tag{14}$$

where $\gamma=1.4$ and $\sigma=0.7$ for atmospheric air are used. The value of Q_{th} turned out to be 39, in good agreement with the present experimental result $Q=36$.

The value of Q_f has been already evaluated to be 25 as the ratio of the resonance frequency f_0 to the width Δf in the frequency response curve shown in Fig. 2. This is 30% less than $Q=36$ obtained above and is significantly different from Q and Q_{th}. Hence, we find that the conventional method does not lead to a correct Q value of the resonator, even when the response curve is well fitted to a Lorentz curve as shown in Fig. 2.

The quality factor obtained from the conventional method may be interpreted [16] as

$$Q_f = \omega\frac{E_S}{\dot{E} + \dot{E}_{loss}}, \tag{15}$$

where $\dot{E}_{loss}$ (>0) represents the dissipative power of the driver. Equation (15) indicates that the conventional method gives the Q value of the combined resonator-driver system and that it becomes equal to the Q value of the resonator when $\dot{E}_{loss}$ is negligibly small in comparison with $\dot{E}$. Therefore, we conclude that the present method has a great advantage over the conventional method, because the Q value of the resonator is directly and reliably obtained without worrying about the presence of the dissipative power $\dot{E}_{loss}$ of the driver.

B. Q value of an acoustic resonator with a load

The ceramic catalyst was inserted as an acoustic load into the resonator at $X=0.46$, where a velocity maximum is formed. The pressure p_e at the closed end was kept at $p^*=782$ Pa. The resulting axial distributions of p and v are found to be very close to those without the load. However, we found a great change in the phase ϕ when the load is installed in the resonator.

The phase ϕ with and without the acoustic load is shown in Fig. 7(a), where the load is illustrated by hatches. The phase ϕ approaches a traveling-wave phase in the region between the driver and load, whereas ϕ remains the standing-wave phase in the region between the load and closed end. This leads to the enhancement of the acoustic intensity only in the region before the load ($X<0.46$).

The acoustic intensity $\bar{I}$ with the load is shown in Fig. 7(b), together with that in the absence of the load. We see that $\bar{I}|_{X=0}$ at the inlet of the resonator is increased to 105 W/m^2, which is 3.6 times larger than that without the load. The additional acoustic intensity is equal to the difference $\Delta\bar{I}=76$ W/m^2 between both ends of the load. This represents the dissipative power due to the load.

The value of $\omega\tau_\nu$ of the present load is 3.8, which is quite small. Furthermore, the acoustic load is placed at the velocity antinode, where the velocity v takes a maximum whereas the pressure p takes a minimum. Therefore, the difference $\Delta\bar{I}$ in

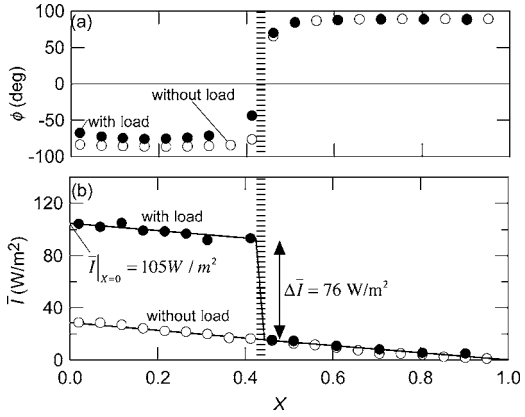

FIG. 7. Axial profile of (a) the phase lead ϕ of V to P and (c) the acoustic intensity $\bar{I}$ in the acoustic resonator with (●) and without (○) the acoustic load. A hatched region represents the load. The acoustic intensity without the load is reproduced from Fig. 6.

the load can be attributed to a viscous loss, because the energy loss due to the thermal conduction is very small, since it is proportional to p^2 as shown in Eq. (12). On the other hand, the slope $\nabla\bar{I}$ outside the load remains the same as that without the load, which means the dissipative powers outside the load are not changed upon the installation of the load. This is because the axial distribution of p and v in the loaded resonator is the same as that shown in Fig. 6(a).

By inserting $\bar{I}|_{X=0}=105$ W/m^2 into Eq. (9), we obtained $\dot{E}=36$ mW as the total input power to the loaded resonator. The acoustic energy $E_s=0.39$ mJ stored in the resonator without the load is also used as that in the loaded resonator, since the axial distribution of p and v is the same as that in the absence of the load. As a result, we obtained $Q=9.5$ in the loaded resonator, which is much smaller than $Q=36$ without the load. As is already mentioned in the Sec. II A, the quality factor Q_f of the loaded resonator was 9.9 in the conventional method. It is important to note that, in the loaded resonator, a better agreement is achieved between the Q values derived from the conventional and the present methods.

In the loaded resonator, the energy loss $\dot{E}=36$ mW is much larger than $\dot{E}=10$ mW without the load, because of the strong viscous dissipation in the load. If Q_f is given as in Eq. (15), it is a natural consequence that Q_f approaches Q defined in Eq. (1) when $\dot{E}$ becomes so large that $\dot{E}_{loss}$ can be neglected. In other words, Q_f becomes approximately equal to the Q of the resonator when the dissipative power in the driven system is large enough relative to that of the driver. Therefore, the better agreement between the Q values obtained from two different methods is due to the strong dissipation in the loaded resonator. However, the conventional method becomes inapplicable when $\dot{E}$ is very large, since the response curve is no longer approximated by a Lorentz peak. On the other hand, it is obvious that the present method can be used even when the response curve does not show a peak due to the strong dissipation, which is another advantage over the conventional method.

IV. SUMMARY

We simultaneously measured the acoustic pressure $P=p\exp(i\omega t)$ and the axial velocity $V=v\exp\{i(\omega t+\phi)\}$ in the resonator, and mapped out spatially where in the resonator the acoustic energy is stored and where it is dissipated. The Q value of the acoustic resonator was then determined using the energy loss $\dot{E}$ and the stored energy E_s in the resonator. We have shown that $Q=36$ thus obtained is in good accordance with the theoretical value ($Q_{th}=39$), but is significantly different from $Q_f=25$ derived from the frequency response curve. Also, we could evaluate $Q=9.5$ of the loaded acoustic resonator, where $Q_f=9.5$ was obtained from the frequency response curve. A better agreement between Q and Q_f is due to the presence of the strong viscous dissipation in the acoustic load. The present method can provide an accurate Q value of the resonator regardless of the degree of the damping in the resonator and the driver.

[1] A. D. Pierce, *Acoustics: An Introduction to Its Physical Principles and Applications* (Acousical Society of America, Woodbury, NY, 1991).
[2] L. E. Kinsler, A. R. Frey, A. B. Coppens, and J. V. Sanders, *Fundamentals of Acoustics* (Wiley, New York, 1999).
[3] T. Yazaki and A. Tominaga, Proc. R. Soc. London, Ser. A **454**, 2113 (1998).
[4] H. Bailliet, P. Lotton, M. Bruneau, V. Gusev, J. C. Valiere, and B. Gazengel, Appl. Acoust. **60**, 1 (2000).
[5] T. Biwa, Y. Ueda, T. Yazaki, and U. Mizutani, Cryogenics **41**, 305 (2001).
[6] T. Yazaki, A. Iwata, T. Maekawa, and A. Tominaga, Phys. Rev. Lett. **81**, 3128 (1998).
[7] T. Yazaki, T. Biwa, and A. Tominaga, Appl. Phys. Lett. **80**, 157 (2002).
[8] T. Biwa, Y. Tashiro, U. Mizutani, M. Kozuka, and T. Yazaki, Phys. Rev. E **69**, 066304 (2004).
[9] Y. Ueda, T. Biwa, U. Mizutani, and T. Yazaki, Appl. Phys. Lett. **81**, 5252 (2002); J. Acoust. Soc. Am. **115**, 1134 (2004).
[10] A. Tominaga, Cryogenics **35**, 427 (1995); *Fundamental Thermoacsoustics* (Uchida Roukakuho, Tokyo, 1998).
[11] L. D. Landau and E. M. Lifshitz, *Fluid Mechanics* (Butterworth-Heinemann, Oxford, 1987).
[12] G. W. Swift, *Thermoacoustics: A Unifying Perspective for Some Engines and Refrigerators* (Acoustical Society of America, Sewickley, PA, 2002).
[13] P. H. Ceperley, J. Acoust. Soc. Am. **66**, 1508 (1979); **72**, 1688 (1982); **77**, 1239 (1985).
[14] G. Petculescu and L. A. Wilen, ARLO **3**, 71 (2002).
[15] G. W. Swift, J. Acoust. Soc. Am. **84**, 1145 (1988).
[16] A. M. Fusco, W. C. Ward, and G. W. Swift, J. Acoust. Soc. Am. **91**, 2229 (1992).